



Design and Research of Triboelectric Energy Harvester for Low Frequency Nonlinear Vibration

Yinqiang Huang¹, Huajiang Ouyang², and Zihao Liu¹(✉)

¹ The Mechanical and Electrical Engineering College, Hainan University, Haikou, China
fageiliuzihao@126.com

² School of Engineering, University of Liverpool, Liverpool L69 3GH, UK

Abstract. Although great progress has been made in the study of triboelectric energy harvesting, most of the efforts are aimed at the manufacturing and experimental demonstration of the harvesters. For simultaneous energy harvesting and vibration control, there is still a strong need of structural design and in-depth theoretical research of structural dynamics of triboelectric harvesters.

In this paper, a harvester in the form of a cantilever beam and two curved surfaces as constraints is proposed. When the cantilever beam vibrates under a low-frequency excitation, the contact between the cantilever beam and one of the curved surfaces is gentle and gradual. Compared with a triboelectric harvester working in the traditional contact-separation mode, this contact can achieve energy harvesting while avoiding the introduction of vibro-impact of the structure, but introduces complex nonlinear vibration. Through the planar rigid body kinematics and a quasi-static analysis, the differential equation of motion for the cantilever beam including the ninth-order geometric nonlinearity for the contact is established. The mathematical model for combining the structural dynamics and electrical dynamics is established. Finally, the approximate analytical solution of the model is obtained by using the harmonic balance method, and the stability of the model under different structural parameters is analyzed by Floquet theory.

Numerical simulation results show that when the frequency excitation is 5.72 Hz, the peak output voltage is 6.9 V and the average power is 1.9 μ W. When the frequency is between 5.72 Hz and 5.93 Hz, the response exhibits bifurcation. Compared with the traditional cantilever beam absorber, the frequency response curve of this structure is deflected due to the nonlinear factors brought about by the curved surface, and the frequency band of vibration hysteresis is narrow. The broadband capacity of the nonlinear spring is proven in the frequency domain for two chosen surface curvature orders, with one low and one high amplitude of excitation. Therefore, the structure proposed in this paper can maintain a larger amplitude in the broadband, thus playing a role in broadening the working frequency band of vibration absorption. In summary, the structure can not only realize vibration energy harvesting without hard impact, but also work as a vibration absorber with nonlinear characteristics.

Keywords: Triboelectric Energy Harvester · Nonlinear cantilever beam · Nonlinear vibration absorber · Nonlinear dynamics · Nonlinear modeling

1 Introduction

Wireless sensor networks have been widely used in various fields, including aerospace engineering, intelligent transportation, smart factories, and other distributed environments, to perform sensing tasks. However, the energy supply for these sensors presents some challenges. These challenges include the use of complex wired power supply systems, limitations of battery power, high maintenance costs, and environmental pollution problems. Additionally, the ambient often contains significant vibrations, such as those produced by mechanical equipment and engineering structures that are commonly used in the industrial and transportation industries. These vibrations can cause significant harm, leading to economic losses and even casualties. Hence, there is an increasing need for vibration control solutions. Moreover, such environment often exhibits low-frequency and broadband vibrations. Therefore, it is imperative to investigate how to effectively harness this mechanical vibration energy to simultaneously power the sensors and control vibration responses. However, there is limited research that focuses on both functions.

Vibration-based energy harvesters offer a promising solution to recycle and utilize the wasted mechanical energy in the environment by converting it into electrical energy. In recent years, piezoelectric [1–4] and electromagnetic [5–7] energy harvesters have been extensively studied. Since the introduction of this concept in 2012 [8], triboelectric energy harvesters (TEHs) have also gained widespread attention due to their unique characteristics. TEHs are self-powered systems that collect energy from environmental vibrations. They offer advantages such as cost efficiency, high energy conversion rates, lightweight, small size, and wide availability of materials [9]. These characteristics make TEHs particularly suitable for collecting low-frequency vibration energy. With their structural design flexibility, TEHs have an immense potential as a replacement for traditional energy supplies in engineering applications.

Electrical charges in TEHs are generated by the friction or contact between triboelectric materials. When two thin organic/inorganic films with distinct surface electron affinities come into contact or undergo separation in the normal direction or sliding in the tangential direction, triboelectrification and electrostatic induction occur. This leads to the generation of an electric potential difference due to the relative motion caused by a mechanical force. As a result, electrons on the surfaces of the two materials are driven to flow between the two electrodes [10]. TEHs typically operate in four working modes: vertical contact-separation mode [11], lateral sliding mode [12], single-electrode mode [13], and free-standing triboelectric-layer mode [14].

TEHs can be widely used for collecting various types of energy in various environments, such as wind energy, water energy, and mechanical energy. Here, some designs will be reviewed briefly. Fu et al. [15] collected vibration energy through triboelectricity generated by the vibration and impact between three parallel cantilever beams. Zhao et al. [16] proposed a novel cantilever type TEH for low-frequency vibration energy collection. In this design, the free end of the cantilever beam is attached to a contact plate with a polytetrafluoroethylene film. When the cantilever beam vibrates upwards, the contact plate is pushed to separate from the top plate, resulting in the generation of triboelectric electricity. Typically, the working mode of a triboelectric energy harvester is separate. However, with further research, mixed working mode TEHs and hybrid TEHs

have also been proposed. Zhao and Ouyang [17] introduced an integrated horizontal sliding and contact separation triboelectric energy harvester. This design includes a slider embedded inside a capsule-structure THE. Under external excitation, the slider produces sliding friction and vibro-impact with the inner wall of the capsule, thereby generating electricity. Currently, most research on THEs has focused on the preparation, experimentation, and surface treatment of triboelectric materials. Research has demonstrated that patterned triboelectric surfaces have higher energy generation efficiency than patternless ones [22]. Various surface patterns have been fabricated and studied, including pyramid and cube patterns [23], nanowire arrays [24], and nanopores [25]. The exploration of triboelectric materials has greatly improved the power generation efficiency and provided new directions for blue energy harvesting.

The use of nonlinearity to expand the resonant bandwidth of a vibration energy harvester has received widespread attention. In addition to the above research, Wang et al. [26] investigated a Piezoelectric energy harvester that utilized a cantilever beam and two symmetric surfaces with given geometry. Similarly, Kluger et al. [7] used a similar structure to an electromagnetic vibration energy harvester to capture vibration energy generated during walking. Nonlinearity has proven to be influential not only in the field of vibration energy harvesting but also in vibration control. Silva et al. [27] applied geometrically nonlinear passive dampers to the main vibration system, and their results showed that the proposed device had a broad frequency response, indicating its ability to effectively engage in targeted energy transfer suitable for applications like vibration attenuation. Despite the extensive study of the vibration energy harvesters with a geometrically nonlinear clamping cantilever structure, this particular structure has not yet been exploited for triboelectric energy harvesting. The properties and contact mode of the contact surfaces play a crucial role in triboelectric harvesting, thus the characteristics of geometrically nonlinear surfaces hold considerable significance and warrant further investigation.

This paper proposes a nonlinear surface contact cantilever triboelectric energy harvester (NSCCTEH) and offers the following scientific contributions for triboelectric energy harvesting. Firstly, the NSCCTEH is theoretically investigated for the first time in triboelectric energy harvesting encompassing structural dynamics and electrodynamic coupling. In contrast to the traditional “separation and closing” mode, this structure exhibits a gradual separation and gradual contact process. Secondly, unlike traditional TEH that typically has the function of only energy harvesting, the proposed NSCCTEH structure can simultaneously perform energy harvesting and vibration control under excitation. Thirdly, this paper expands the resonant bandwidth by incorporating geometric nonlinearity, resulting in a deflection of the frequency response curve. Consequently, a larger amplitude is maintained within a wider frequency band, achieving the goal of expanding the working frequency band. To better demonstrate these characteristics, the paper provides the derivation of the structural dynamics model and stability analysis of the structure, followed by the analysis of the equivalent electrical model. Finally, the paper discusses the dynamic response and the power output, and the influencing parameters.

2 Prototype Design

The proposed TEH in this paper consists of two parts: one is a nonlinear spring resulting from a cantilever beam constrained between two curved surfaces; the other part consists of a generator set which includes a polytetrafluoroethylene film (PTFE) and a metal film (Cu) covering the two curved surfaces and a cantilever beam made of copper. The unique structure improves the dynamic performance by the variable-curvature curved surfaces, such as preventing secondary vibration caused by impact-contact of the absorber, minimizing friction by reducing the relative sliding between the cantilever beam and the curved surface, and inhibiting excessive deflection of the cantilever beam by the curved surface. In a word, the proposed structure is a kind of vibration energy harvester and also is a nonlinear vibration absorber.

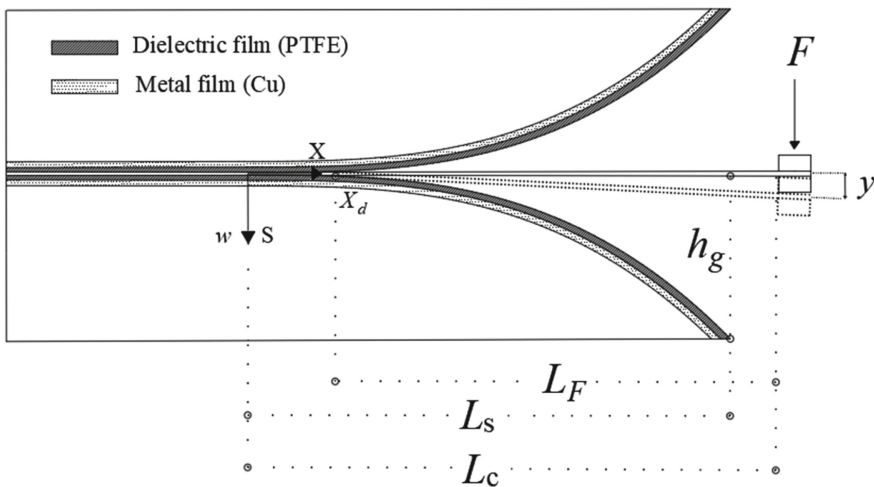


Fig. 1. Simplified model. where L_C is the cantilever length, h_g is the gap between the surface end and the undeflected cantilever, and L_S is the length of the surface in the x direction, x_d is the demarcation point, L_F is the length of the un-contact part of the cantilever in the x direction; The tip displacement y of the beam depends on the vertical force F and the shape of the contact surface.

2.1 Quasi-Static Analysis

The structural configuration of the TEH is described in Fig. 1, where two variable-curvature surfaces grip a cantilever beam with a mass at another end of the beam. The unique variable-curvature surface design of the TEH ensures that the curvature radius on the surface is maximum at the root and decreases along its length. In contrast, the curvature radius of the free cantilever beam at the base is minimum and increases along its length. This opposite trend in the variation of curvature radii along the beam length allows for immediate contact between the beam and the surface even with minimal force

applied. The contact area between the cantilever beam and the surface gradually increases as the beam deforms. The improved surface shape can be represented as follows:

$$S = h_g \left(\frac{x}{L_S} \right)^n \quad (1)$$

where L_S is the length of the surface in the x direction; h_g is the distance between the undeflected cantilever beam and the curved surface at $x = L_S$; n is an integer number greater than 2 to ensure that the curvature radius at the root of the surface is 0. Any one of the two curved surfaces act as a nonlinear spring. To determine the characteristics of the nonlinear springs, it is necessary to obtain the force-displacement relationship. For this purpose, a vertical force F is applied at the end of the cantilever beam. The tip displacement y of the beam depends on the vertical force F and the shape of the contact surface. It can be divided into three components: $y = y_1 + y_2 + y_3$. The first component y_1 is the displacement caused by the bending of the non-contact part of the cantilever beam. The second component y_2 is due to the rotation of the beam segment (from x_d to L_S) at the contact boundary point x_d , The third component y_3 is the deflection of the beam at the contact boundary point x_d , Therefore, the displacement y of the cantilever beam tip under the action of external force F is:

$$y = y_1 + y_2 + y_3 = \frac{FL_F^3}{3EI} + \left. \frac{dS}{dx} \right|_{x=x_d} \cdot L_F + S(x_d) \quad (2)$$

The relationship between the length of the contact boundary point x_d and the restoring force F_R :

$$F_R = \frac{E I h_g}{L_S^n} n(n-1) \frac{x_d^{n-2}}{L_C - x_d} \quad (3)$$

For a detailed derivation of tip displacement y and restoring force F_R , please refer to [26]. The change of nonlinear spring force F_R with displacement y of the tip of the cantilever beam is shown in Fig. 2(a). When the cantilever is gradually bent along the curved surface, the relationship between the contact length of the beam and the displacement of the beam tip under different curvature orders is shown in Fig. 2(b). In all cases, the maximum contact length between the cantilever occurs at the maximum displacement of the beam tip and its value is bounded. Near the the clamped boundary, with the increase of parameter, n , the contact length suddenly increases, and then, with the increase of displacement, the contact length gradually increases until the maximum contact length is reached. In this process, compared with different parameter values of n , The contact length for parameter $n = 5$ is greater than the contact lengths for the other two parameters, n , under small deformation conditions of the cantilever beam. As the tip displacement, y , increases to around 0.06 m, the contact lengths for all three parameters gradually intersect until they reach the same maximum contact length. This suggests that, in the structures discussed in this chapter, surfaces with higher values of n are more suitable for use as TEH. This is because even with small tip displacements, larger contact lengths (contact area) can be achieved. Additionally, the maximum curvature bending on the cantilever beam can be controlled, and the maximum normal stress on the beam can be kept within a certain value under any external force. This effectively prevents structural damage under extreme excitation.

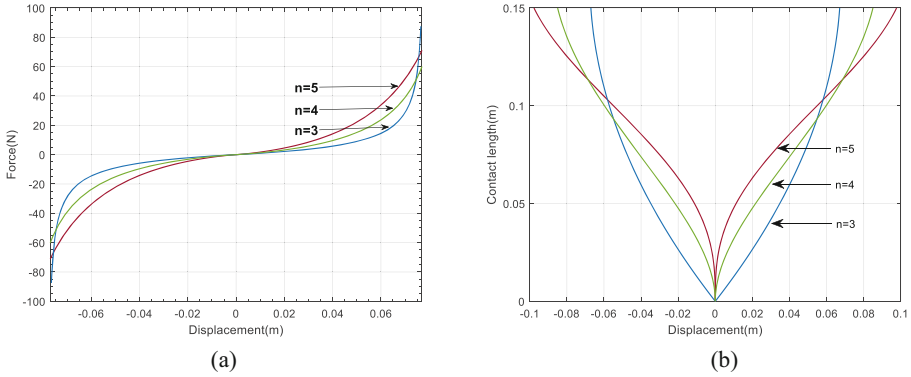


Fig. 2. The relationship between restoring force and tip displacement (a) and the relationship between contact length and tip displacement (b) under different n values

3 Structural Dynamics Model

In this section, a structural dynamics model is established to comprehensively study the dynamic response of several nonlinear springs composed of different curvature surfaces and cantilever beams under simple harmonic base excitation. Numerical simulation is utilized to explore the influence of various parameters on vibration characteristics and conduct stability analysis of periodic solutions.

3.1 Approximate Analytical Solution

Assuming that the system is driven by external excitation, the excitation function $u_b = A \cos(\omega_b t)$, where A and ω_b represent the excitation amplitude and the excitation frequency, respectively. The dynamic equations of the system are numerically solved using the Matlab differential equation solver ode45, which uses a variable step size and implements the Runge-Kutta algorithm, suitable for solving nonstiff differential equations. The equation governing the lateral motion of the beam is:

$$m\ddot{y}(t) + c\dot{y}(t) + F_R = -m\ddot{u}_b \quad (4)$$

where m is the equivalent mass of the tip mass and the cantilever beam mass, and c is the mechanical damping coefficient.

The next step is to determine the approximate expression of the nonlinear resilience F_R of Eq. (2), which is found to be through curve-fitting:

$$F_R = k_L y + k_{NL} y^9 \quad (5)$$

where k_L and k_{NL} are linear and nonlinear stiffness coefficients, respectively.

3.2 Non-dimensionalization

Based on the resulting nonlinear restoring force F_R , substituting Eq. (5) into Eq. (4) can represent a new differential equation expression:

$$m\ddot{y}(t) + c\dot{y}(t) + k_L y + k_{NL} y^9 = -m\ddot{u}_b \quad (6)$$

The relative contribution of constant terms in Eq. (6) must be evaluated through nondimensionalization. By scaling the time variable by a characteristic time, T_c , let:

$$\tau = \frac{t}{T_c}, \quad \mu = y, \quad \mu' = T_c \dot{y}, \quad \mu'' = T_c^2 \ddot{y} \quad (7)$$

where $T_c = \sqrt{\frac{m}{k_L}}$, substitute Eq. (7) into (6), and simplify to get:

$$\mu'' + \lambda \mu' + \mu + \varepsilon \mu^9 = \Lambda \Omega_r^2 \cos \Omega_r \tau. \quad (8)$$

where:

$$\lambda = \frac{c}{\sqrt{mk_L}}, \quad \varepsilon = \frac{k_{NL}}{k_L}, \quad \Omega_r = \omega_b \sqrt{\frac{m}{k_L}} \quad (9)$$

3.3 System Response Near Resonance

Because there are higher-order terms in Eq. (8), it is difficult to obtain a solution in a closed form, so an approximate solution is sought by the harmonic balance method, which is suitable for systems with polynomial nonlinear terms. A solution to Eq. (8) is assumed to have a single frequency of the form:

$$\mu(t) \approx \mu_h = A \cos(\Omega_r \tau) + B \sin(\Omega_r \tau) \quad (10)$$

where A and B are Fourier coefficients. The interest is in the low-frequency behaviour. The detailed derivation process is mathematically extensive and produces very long expressions. Therefore, this article briefly describes some of the steps of the process. Substituting Eq. (10) into Eq. (8) gives the power expressions of sine and cosine, and then through a series of trigonometric manipulations (e.g., $\sin(\Omega_r \tau)^3 = \frac{1}{4} \sin(3\Omega_r \tau) + \frac{3}{4} \sin(\Omega_r \tau)$), an expression with the highest harmonic ($9\Omega_r \tau$) is obtained. After ignoring all higher-order harmonic terms greater than ($3\Omega_r \tau$) due to their tiny coefficients, the following solutions can be derived [27]:

$$A - \Omega_r^2 A + \frac{63}{128} \varepsilon A^9 + \frac{189}{64} \varepsilon B^4 A^5 + \frac{63}{32} \varepsilon B^2 A^7 + \Lambda \Omega_r^2 + \frac{63}{128} \varepsilon B^8 A + \frac{63}{32} \varepsilon B^6 A^3 + B \Omega_r \lambda = 0 \quad (11)$$

$$B + \frac{63}{128} B^9 \varepsilon - B \Omega_r^2 + \frac{189}{64} A^4 B^5 \varepsilon + \frac{63}{32} A^6 B^3 \varepsilon + \frac{63}{128} A^8 B \varepsilon - A \Omega_r \lambda + \frac{63}{32} A^2 B^7 \varepsilon = 0 \quad (12)$$

Substituting $A = a \cos(\theta)$, $B = b \sin(\theta)$ into Eq. (11) and Eq. (12) for a polar substitution, and then eliminating the trigonometric term through some techniques, and performing a series of combined simplifications, the relationship between frequency and amplitude is finally obtained:

$$\frac{3969}{16384} a^{18} \varepsilon^2 - \frac{63}{64} a^{10} \varepsilon \Omega_r^2 + \frac{63}{64} a^{10} \varepsilon + a^2 \Omega_r^4 - 2a^2 \Omega_r^2 + a^2 + \lambda^2 a^2 \Omega_r^2 = \Lambda^2 \Omega_r^4 \quad (13)$$

4 Electric Model of Triboelectric Energy Harvester

As shown in Fig. 3, the design proposed in this paper consists of two independent triboelectric energy harvesters, that is, the upper and lower surfaces of the entire structure with the beam form two TEHs in contact-separation mode, represented by TEH1 and TEH2, respectively. For TEH_{*i*}, the equivalent model includes an open-circuit voltage V_{oci} and variable capacitance C_i , which are assumed to be only functions of the relative displacement between the beam and the surface, independent of other motion parameters such as velocity and acceleration [28]. Because of the symmetrical surface structure used in this design, TEH2 and TEH1 have identical dynamic behaviour. And the relationship between contact length x_d and displacement y has been obtained in quasi-static analysis. So, the equivalent model of TEH1 and TEH2 includes the open circuit voltage V_{oci} and variable capacitance C_i combined into one expression, that is, the equivalent capacitance C and the open circuit voltage V_{oc} (Fig. 4).

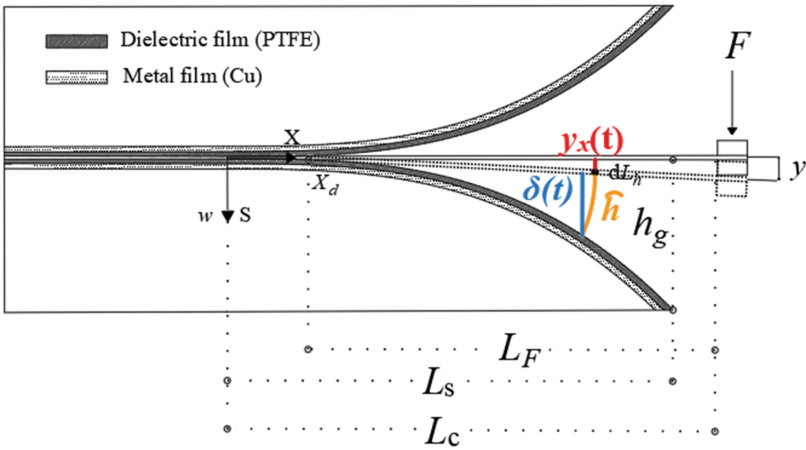


Fig. 3. Simplify electrical models

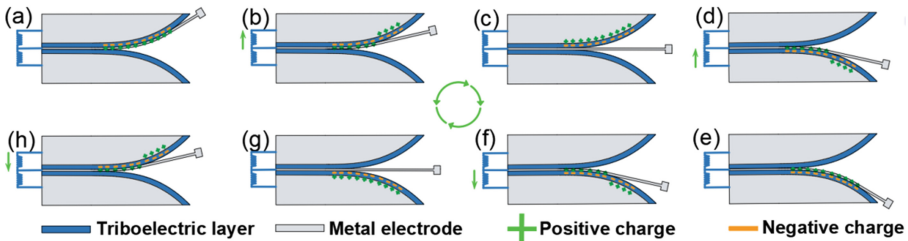


Fig. 4. Working cycle of triboelectric pair.

In order to determine the capacitance C and open circuit voltage $V_{oc} = V_a + V_d$ of the system, considering a capacitor of infinitesimal length dL_h , one can get the infinitesimal

capacitance of the TEH for a given distance. Upon integration over the length, the total capacitance between two electrodes can be obtained, and the electromechanical model can be established accordingly [31]. Reviewing the quasi-static analysis in Sect. 2.1, it can be seen that the relative displacement function of the infinitesimal length dL_h and the corresponding surface on the cantilever beam can be rewritten in Eq. (1) as:

$$S_x = h_g \left(\frac{L_h}{L_s} \right)^n \quad (14)$$

where S_x is the distance from any point on the untouched surface to the x -axis, $L_h = x_d \rightarrow x_{dMax}$ is the distance range from the contact point of the beam and the surface to the longest contact point, and then rewrite equation Eq. (2) as:

$$y_x(t) = \frac{h_g x_d^{n-2}}{3L_s^n} (3x_d^2 + 3nx_d(L_h - x_d) + n(n-1)(L_h - x_d)^2) \quad (15)$$

where $y_x(t)$ expresses the deflection of any different elements on the cantilever beam of the lower separation part at a certain time. The vertical distance between the corresponding different infinitesimal length dL_h of the cantilever and the surface separation part can be expressed as:

$$\delta(t) = S_x - y_x = \frac{3h_g L_h^n - h_g x_d^{n-2} (3x_d^2 + 3nx_d(L_h - x_d) + n(n-1)(L_h - x_d)^2)}{3L_s^n} \quad (16)$$

For TEH_i, the equivalent capacitance C can be divided into two capacitance components, where the free cantilever part and the surface non-contact part are non-parallel plate capacitors $C_{i.1}$, the cantilever and surface contact parts are equivalent to the parallel plate capacitance $C_{i.2}$, and the potential difference V_d inside the dielectric layer, which are expressed as:

$$C = C_{i.1} + C_{i.2} \quad (17)$$

$$C_{i.1} = \int_{x_d}^{x_{dMax}} \frac{\epsilon_0 b}{d_s + \delta} dL_h, C_{i.2} = \frac{\epsilon_0 A_c}{d_s} \quad (18)$$

$$V_d = -\frac{\sigma_s d_s}{\epsilon_0} \quad (19)$$

where $d_s = \frac{d_1}{\epsilon_{rs}}$ is the effective thickness of the PTFE film, d_1 is the thickness of the PTFE film, ϵ_{rs} is the relative permittivity, $A_c = x_d b$, represents the area of the contact part, $A_b = (x_{dMax} - x_d)b$, represents the area of the untouched part, b is the beam width, σ_s is the surface density of the frictional charge, ϵ_0 is the vacuum permittivity, and x_{dMax} is the maximum contact length.

Since the free cantilever plates are not parallel to the PTFE on the curved surface, the potential difference V_a between the two plates cannot be calculated a simple shunt capacitor model. In this model, the V_a is estimated by considering the electric field energy of the region between the free cantilever plate and the PTFE. It should be noted that the potential difference between the free cantilever plate and the PTFE at each position along the length direction is equal. In other words, the free cantilever plate and the dielectric layer are actually two equipotential planes to which the electric field lines

should be perpendicular. After finding the arc length \widehat{h} corresponding to each differential infinitesimal length dL_h , the total electric field energy W can be expressed as:

$$W = \int_{x_d}^{x_{dMax}} \frac{1}{2} \varepsilon_0 E_a^2 dv = \int_{x_d}^{x_{dMax}} \frac{1}{2} \varepsilon_0 \left(\frac{V_a}{h} \right)^2 \widehat{h} dL_h = \frac{1}{2} \varepsilon_0 V_a^2 b \int_{x_d}^{x_{dMax}} \frac{1}{h} dL_h \quad (20)$$

where E_a is the electric field strength between the two plates, v is the volume of space gap, combined with the electric field energy formula $W = \frac{C_{i,1} V_a^2}{2}$, after a series of simplifications, V_a expression is shown:

$$V_a = \frac{\sigma_s (x_{dMax} - x_d)}{\varepsilon_0 \int_{x_d}^{x_{dMax}} \frac{1}{h} dL_h} \quad (21)$$

The electricity generation equation of the triboelectric harvesters can be written as:

$$V = -\frac{Q}{C} + V_{oc} \quad (22)$$

Applying Ohm's law on Eq. (22), one can get the electric differential equation as:

$$R \frac{dQ}{dt} + \frac{Q}{C} - V_{oc} = 0 \quad (23)$$

For continuous motion, the electric output signal from the harvesters is also time-dependent. In such a case, the average output power is used to assess the performance of vibration-based energy harvesters [10]. The corresponding average output power \overline{P} for TEHi and the total average power \overline{P} can be obtained by:

$$\overline{P} = \frac{\int_0^t V^2(t) dt}{Rt} \quad (24)$$

5 Numerical Simulations and Results

Figure 5 shows the amplitude-frequency response curves of the harmonic balance solution and the numerical solution, and the amplitude of the system can be determined at this frequency when the displacement reaches a steady state under the sweeping excitation of each frequency step and equal amplitude. As shown in Fig. 5(a), there is a stable solution to the steady-state response in the range of frequencies less than 5.72 Hz; when the frequency is in the range of 5.72 Hz–5.93 Hz, the response bifurcates, and the system has two stable solutions and one unstable solution. In Fig. 5, it is clear that the main formant is shifted towards the high frequency, and the jump occurs to the right of the formant. As can be seen from Fig. 6(a), as the excitation amplitude increases, the jump frequency of the system increases, the unstable frequency range and the main resonance frequency range also increase, and the degree of bending of the frequency response curve increases. It can also be seen from the figure that the frequency response curve is bent due to nonlinearity, and there are multi-value regions in the above figure, which is also the cause of the jumping phenomenon. The stability of the system is also verified by the evolution of the Floquet multiplier in Fig. 6(b), where the Floquet multiplier evolves as the excitation frequency increases. The frequencies at which the Floquet multiplier

leaves and re-enters from the unit circle are 5.72 Hz and 5.93 Hz, respectively, which are also consistent with the numerical simulation and approximate analytical solution in Fig. 5. Figure 7 shows the simulation results of the contact length, displacement, and output voltage of the acquirer with a surface order $n = 3$ under the excitation of an external resistor of $10 \text{ M}\Omega$ under the excitation of the resonance frequency of 5.72 Hz and the excitation amplitude $\Lambda = 1.2 \text{ mm}$. The simulated output voltage is 6.9 V peak and the average output power is $1.9 \mu\text{W}$. Future work will involve parameter optimization, including the surface width, surface parameter n , cantilever length; and nano-treatment of contact surfaces. In addition to the current geometrically nonlinear structure, other nonlinear factors such as magnetic nonlinearity will also be introduced.

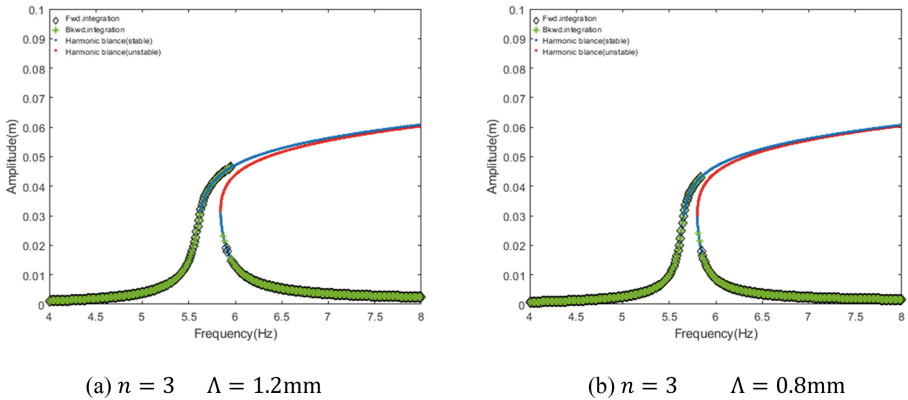


Fig. 5. Harmonic balance method and numerical solution of amplitude-frequency response under different conditions are applied

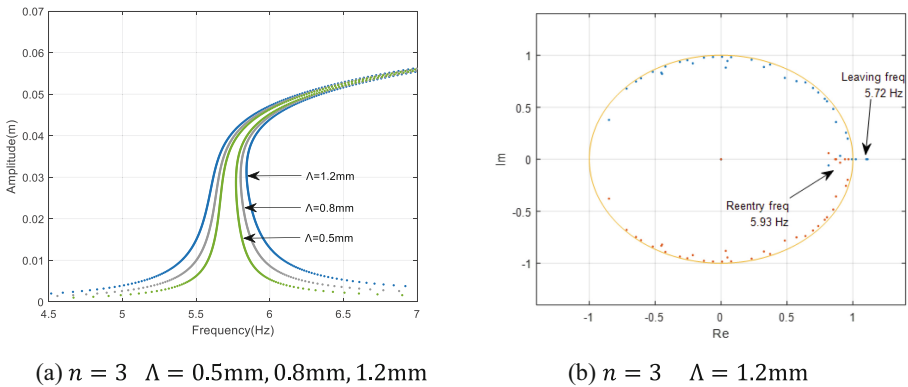


Fig. 6. (a) The relationship between the response of the system and the amplitude of the excitation under the same curvature order. (b) Evolution of stability

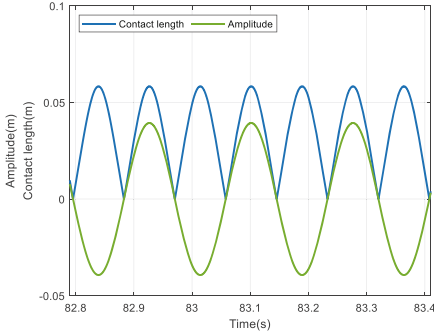
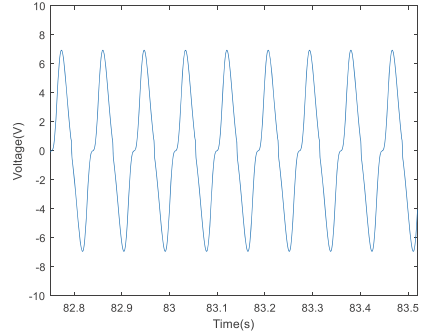
(a) $n=3$ $\Lambda = 1.2\text{mm}$ (b) $n=3$ $\Lambda = 1.2\text{mm}$

Fig. 7. (a) The amplitude of the beam tip and the contact length between the beam and the surface over time (b) THE output voltage waveform

6 Conclusions

This paper proposes a NSCCTEH which avoids the vibro-impact working characteristics of the design and greatly increases the service life due to low friction. It can be vibrated under low-frequency excitation force, and the contact between the cantilever beam and the curved surface is a relatively gentle gradual contact. This method achieves energy harvesting while avoiding vibro-impact. However, it also introduces relatively complex nonlinear vibration. In this paper, the first step is to establish a dynamic differential equation containing a ninth-order geometric nonlinearity through planar rigid body kinematics combined with quasi-static analysis. The structural coefficients are then designed using parameter identification. The next step is to obtain the approximate analytical solution of the model using the harmonic balance method and analyze the stability of the model under different structural parameters using Floquet theory. Finally, a coupled mathematical model of structural dynamics and electrostatics is established. This paper presents the first theoretical study of the nonlinear surface contact cantilever triboelectric energy harvester. It includes investigations into structural dynamics and electrical analysis. This study is essential for the efficient design and manufacture of energy harvesters.

Through numerical simulation, the dynamic behavior and electrical output performance of the triboelectric energy harvester (TEH) were studied. It was discovered that the introduction of a geometric nonlinear contact surface benefits the TEH by enabling it to maintain a large steady-state amplitude in a wide frequency band. This expansion of the working frequency band allows for greater vibration absorption. Furthermore, even without the traditional contact separation typically used to increase electrical output, the TEH still demonstrates a relatively good electrical output. Unlike other vibration-based energy harvesters, this unique structure of the TEH avoids the need for new shock excitation while simultaneously maintaining the electrical output characteristics found in both traditional contact separation and horizontal sliding TEHs. In summary, this structure not only facilitates vibration energy harvesting without the need for shock in

low-frequency vibration environments, but it can also serve as a shock absorber with non-linear characteristics. These findings highlight the potential of the TEH in low-frequency environments for energy harvesting and vibration absorption.

References

1. Madinei, H., Khodaparast, H.H., Adhikari, S., Friswell, M.I.: Design of MEMS piezoelectric harvesters with electrostatically adjustable resonance frequency. *Mech. Syst. Sig. Process.* **81**, 360–374 (2016)
2. Abdelkefi, A., Najar, F., Nayfeh, A.H., Ayed, S.B.: An energy harvester using piezoelectric cantilever beams undergoing coupled bending-torsion vibrations. *Smart Mater. Struct.* **20**, 115007 (2011)
3. Fu, H., Yeatman, E.M.: Rotational energy harvesting using bi-stability and frequency up-conversion for low-power sensing applications: theoretical modelling and experimental validation. *Mech. Syst. Sig. Process.* **125**, 229–244 (2019). <https://doi.org/10.1016/j.ymssp.2018.04.043>
4. Vocca, H., Neri, I., Travasso, F., Gammaitoni, L.: Kinetic energy harvesting with bistable oscillators. *Appl. Energy* **97**, 771–776 (2012)
5. Arroyo, E., Badel, A., Formosa, F., Wu, Y., Qiu, J.: Comparison of electromagnetic and piezoelectric vibration energy harvesters: model and experiments. *Sens. Actuators* **183**, 148–156 (2012)
6. Wang, X., Liang, X., Shu, G., Watkins, S.: Coupling analysis of linear vibration energy harvesting systems. *Freq. Anal. Vib. Energy Harvest. Syst.* **1**(1), 203–229 (2016)
7. Kluger, J.M., Sapsis, T.P., Slocum, A.H.: Robust energy harvesting from walking vibrations by means of nonlinear cantilever beams. *J. Sound Vib.* **341**, 174–194 (2015)
8. Wang, Z.L., Lin, L., Chen, J., Niu, S., Zi, Y.: *Triboelectric Nanogenerators*. Springer, Cham (2016)
9. Jin, C., Kia, D.S., Jones, M., Towfighian, S.: On the contact behavior of micro-/nano-structured interface used in vertical-contact-mode triboelectric nanogenerators. *Nano Energy* **27**, 68–77 (2016)
10. Zhang, C., Wang, Z.L.: *Triboelectric Nanogenerators*. Springer, (2016)
11. Niu, S., et al.: Theoretical study of contactmode triboelectric nanogenerators as an effective power source. *Energy Environ. Sci.* **6**, 3576–3583 (2013)
12. Wang, S., Lin, L., Xie, Y., Jing, Q., Niu, S., Wang, Z.L.: Sliding-triboelectric nanogenerators based on in-plane charge-separation mechanism. *Nano Lett.* **13**, 2226–2233 (2013)
13. Yang, Y., et al.: Single-electrode-based sliding triboelectric nanogenerator for self-powered displacement vector sensor system. *ACS Nano* **7**(8), 7342–7351 (2013)
14. Fu, Y., Ouyang, H., Davis, R.B.: Nonlinear dynamics and triboelectric energy harvesting from a three-degree-of-freedom vibro-impact oscillator. *Nonlinear Dyn.* **92**, 1985–2004 (2018)
15. Fu, Y., Ouyang, H., Davis, R.B.: Triboelectric energy harvesting from the vibro-impact of three cantilevered beams. *Mech. Syst. Sig. Process.* **121**, 509–531 (2019)
16. Zhao, C., Yang, Y., Upadrashta, D., Zhao, L., Lund, H., Kaiser, M.J.: Design, modeling and experimental validation of a low-frequency cantilever triboelectric energy harvester. *Energy* **214**, 118885 (2021)
17. Zhao, H., Ouyang, H.: A capsule-structured triboelectric energy harvester with stick-slip vibration and vibro-impact. *Energy* **235**, 121393 (2021)
18. Yang, J., et al.: Broadband vibrational energy harvesting based on a triboelectric nanogenerator. *Adv. Energy Mater.* **4**(6), 1–9 (2014)

19. Saadatnia, Z., Asadi, E., Askari, H., Esmailzadeh, E., Naguib, H.E.: A heaving point absorber-based triboelectric-electromagnetic wave energy harvester: an efficient approach toward blue energy. *Int. J. Energy Res.* **42**, 2431–2447 (2018)
20. Liu, G., Guo, H., Xu, S., Hu, C., Wang, Z.L.: Oblate spheroidal triboelectric nanogenerator for all-weather blue energy harvesting. *Adv. Energy Mater.* **9**, 1900801 (2019)
21. Jiang, T., et al.: Robust swing-structured triboelectric nanogenerator for efficient blue energy harvesting. *Adv. Energy Mater.* **10**(23), 2000064 (2020)
22. Jin, C., Kia, D.S., Jones, M., Towfighian, S.: On the contact behaviour of micro-/nano-structured interface used in vertical-contact-mode triboelectric nanogenerators. *Nano Energy* **27**, 68–77 (2016)
23. Wang, S.H., Lin, L., Wang, Z.L.: Nanoscale triboelectric-effect-enabled energy conversion for sustainably powering portable electronics. *Nano Lett.* **12**(12), 6339–6346 (2012)
24. Wang, S., Lin, L., Xie, Y., Jing, Q., Niu, S., Wang, Z.L.: Sliding-triboelectric nanogenerators based on in-plane charge-separation mechanism. *Nano Lett.* **13**(5), 2226–2233 (2013)
25. Yang, J., et al.: Broadband vibrational energy harvesting based on a triboelectric nanogenerator. *Adv. Energy Mater.* **4**(6), 1301322 (2014)
26. Wang, C., Zhang, Q., Wang, W., Feng, J.: A low-frequency, wideband quad-stable energy harvester using combined nonlinearity and frequency up-conversion by cantilever-surface contact. *Mech. Syst. Sig. Process.* **112**, 305–318 (2018)
27. Silva, C.E., Gibert, J.M., Maghareh, A., Dyke, S.J.: Dynamic study of a bounded cantilevered nonlinear spring for vibration reduction applications: a comparative study. *Nonlinear Dyn.* **101**(2), 893–909 (2020)
28. Niu, Y.S., et al.: Simulation method for optimizing the performance of an integrated triboelectric nanogenerator energy harvesting system. *Nano Energy* **8**, 150–156 (2014)
29. Krack, M., Gross, J.: *Harmonic Balance for Nonlinear Vibration Problems*. Springer, Cham (2019). <https://doi.org/10.1007/978-3-030-14023-6>
30. Nayfeh, A.H., Balachandran, B.: *Applied Nonlinear Dynamics*, 2nd edn. Wiley-VCH, Weinheim (2004)
31. Boisseau, S., Despesse, G., Ricart, T., Defay, E., Sylvestre, A.: Cantilever-based electret energy harvesters. *Smart Mater. Struct.* **20**(10), 105013 (2011)